

## The Structure and Evolution of Hurricane Elena (1985). Part II: Convective Asymmetries and Evidence for Vortex Rossby Waves

KRISTEN L. CORBOSIERO,\* JOHN MOLINARI, AND ANANTHA R. AIYYER

*Department of Earth and Atmospheric Sciences, University at Albany, State University of New York, Albany, New York*

MICHAEL L. BLACK

*NOAA/AOML/Hurricane Research Division, Miami, Florida*

(Manuscript received 3 October 2005, in final form 1 March 2006)

### ABSTRACT

A portable data recorder attached to the Weather Surveillance Radar-1957 (WSR-57) in Apalachicola, Florida, collected 313 radar scans of the reflectivity structure within 150 km of the center of Hurricane Elena (in 1985) between 1310 and 2130 UTC 1 September. This high temporal and spatial (750 m) resolution dataset was used to examine the evolution of the symmetric and asymmetric precipitation structure in Elena as the storm rapidly strengthened and attained maximum intensity. Fourier decomposition of the reflectivity data into azimuthal wavenumbers revealed that the power in the symmetric (wavenumber 0) component dominated the reflectivity pattern at all times and all radii by at least a factor of 2. The wavenumber 1 asymmetry accounted for less than 20% of the power in the reflectivity field on average and was found to be forced by the environmental vertical wind shear.

The small-amplitude wavenumber 2 asymmetry in the core was associated with the appearance and rotation of an elliptical eyewall. This structure was visible for nearly 2 h and was noted to rotate cyclonically at a speed equal to half of the local tangential wind. Outside of the eyewall, individual peaks in the power in wavenumber 2 were associated with repeated instances of cyclonically rotating, outward-propagating inner spiral rainbands. Four separate convective bands were identified with an average azimuthal velocity of  $25 \text{ m s}^{-1}$ , or  $\sim 68\%$  of the local tangential wind speed, and an outward radial velocity of  $5.2 \text{ m s}^{-1}$ . The azimuthal propagation speeds of the elliptical eyewall and inner spiral rainbands were consistent with vortex Rossby wave theory.

The elliptical eyewall and inner spiral rainbands were seen only in the 6-h period prior to peak intensity, when rapid spinup of the vortex had produced an annular vorticity profile, similar to those that have been shown to support barotropic instability. The appearance of an elliptical eyewall was consistent with the breakdown of eyewall vorticity into mesovortices, asymmetric mixing between the eye and eyewall, and a slowing of the intensification rate. The inner spiral rainbands might have arisen from high eyewall vorticity ejected from the core during the mixing process. Alternatively, because the bands were noted to emanate from the vertical shear-forced deep convection in the northern eyewall, they could have formed through the axisymmetrization of the asymmetric diabatically generated eyewall vorticity.

### 1. Introduction

Corbosiero et al. (2005, hereafter Part I) examined changes in Hurricane Elena's (in 1985) inner-core sym-

metric structure over a 55-h period during which the storm rapidly intensified and then weakened (Case 1986). Through the use of azimuthal and time averages, they found that Elena's changes in intensity were consistent with the axisymmetric intensification mechanism of Shapiro and Willoughby (1982) and the balanced spindown simulations of Montgomery et al. (2001). As noted in Burpee and Black (1989) and Part I however, significant azimuthal asymmetries existed in Elena's inner-core reflectivity structure. These asymmetries included noncircular-shaped eyewalls, a strong north-south dipole in eyewall convection, and propagating

---

\* Current affiliation: National Center for Atmospheric Research, Boulder, Colorado. The National Center for Atmospheric Research is sponsored by the National Science Foundation.

---

*Corresponding author address:* Kristen Corbosiero, National Center for Atmospheric Research, P.O. Box 3000, Boulder, CO 80307.  
E-mail: corbosie@ucar.edu

inner spiral rainbands to the west and southwest of the center.

Understanding the dynamics of the asymmetries in the core of tropical cyclones is of fundamental importance. They influence not only storm structure, but storm motion (Wang and Holland 1996; Nolan et al. 2001) and intensity (Montgomery and Kallenbach 1997; Möller and Montgomery 1999, 2000). In recent years, our knowledge of the interaction between asymmetries and their parent vortices has been greatly advanced by the use of potential vorticity (PV) dynamics and the recognition that PV (or Rossby type) waves can and do exist in the vortex core. These vortex Rossby waves (VRWs) propagate on the radial gradient of mean storm vorticity, analogous to Rossby waves in the large-scale circulation (MacDonald 1968).

The term “vortex Rossby wave,” and a formal theory for the propagation and interaction of the waves with the mean flow, were first presented by Montgomery and Kallenbach (1997) and later generalized by McWilliams et al. (2003). They showed that the axisymmetrization of PV anomalies, such as those generated through moist-convective processes, by the strong horizontal shear of the mean vortex was accompanied by outward-propagating VRWs that accelerated the tangential winds near the radius of wave excitation. Montgomery and Enagonio (1998) and Möller and Montgomery (1999, 2000) used a three-dimensional quasi-geostrophic model and a fully nonlinear asymmetric balance model, respectively, to show that tropical cyclogenesis and intensification could occur through the axisymmetrization and ingestion of like-signed PV anomalies by a parent vortex with a monopole vorticity structure. Furthermore, through the continual injection of PV pulses (to simulate the effects of ongoing convection), Möller and Montgomery (2000) showed that an initially tropical storm-strength vortex could develop a warm core and attain hurricane strength on realistic time scales.

Tropical cyclones exhibiting monopoles of vorticity are, however, likely to occur only during the tropical storm and weak hurricane stages of development, while rapidly intensifying or mature hurricanes with well-developed eyewalls usually exhibit rings of elevated PV on the inner edge of the eyewall (Kossin and Eastin 2001; Mallen et al. 2005). Wang (2001, 2002a,b) showed that the asymmetric structure within 70 km of the center of his modeled vortex with an annular tower of PV was dominated by wavenumber 1 and 2 VRWs. Similar results were found by Chen et al. (2003), who showed that the leading modes in wave activity in the core were VRWs, generated in the lower eyewall through diabatic

heating. The waves were found to be well coupled to convection as the enhanced vertical velocity associated with the wave led to the appearance of inner spiral rainbands (Chen and Yau 2001; Wang 2002b).

Unlike their monopole vortex counterparts discussed previously, numerical simulations of vortices with annular PV rings have failed to document a consistent influence of VRWs on the intensity of the mean vortex. Chen and Yau (2001), Möller and Shapiro (2002), and Chen et al. (2003) documented maximum VRW activity near the radius of maximum wind (RMW), and the transport of high angular momentum and PV by the VRWs radially inward, from the eyewall toward the eye. This inward transport of high vorticity by VRWs was associated with intensification, as the maximum tangential wind spinup occurred just inside the RMW, causing the RMW to propagate inward with time and leading to contraction of the eyewall. On the other hand, Wang (2002b) and Chen and Yau (2003) found VRW–mean flow interactions tended to inhibit strengthening as the VRWs acted to spin up the tangential winds directly in the eye and decelerate the winds at the RMW.

Further complicating the dynamics in storms with elevated rings of vorticity in the eyewall is the possibility of barotropic instability. Schubert et al. (1999) showed that an annular vorticity structure contains counter-propagating VRWs with respect to the flow on its inner and outer vorticity gradients. If these waves became phase locked, they grew in concert and led to the exponential instability of the ring, whereby the eyewall vorticity pooled into discrete areas, creating mesovortices. Depending on the initial conditions of the PV ring, the mesovortices either merged over time and relaxed to a monopole (Schubert et al. 1999; Chen and Yau 2003), or remained separate to form a quasi-steady rotating lattice of vortices that gave the appearance of elliptical (two mesovortices) or polygonal (four or more mesovortices) eyewalls (Kossin and Schubert 2001). In either case, the asymmetric mixing by the mesovortices between the eye and eyewall brought high eyewall vorticity into the eye and low vorticity from the eye outward. To conserve angular momentum during such a rearrangement, some high eyewall vorticity was also mixed outward, taking the form of vorticity filaments, or spiral bands with VRW characteristics (Kuo et al. 1999; Schubert et al. 1999).

Given the copious amount of numerical modeling studies dealing with VRWs in recent years, it is somewhat surprising that only a handful of observational studies have examined convective asymmetries in the core of tropical cyclones and evaluated whether they

exhibit the properties of the VRWs seen in numerical models. Muramatsu (1986) documented 15 h of counterclockwise-rotating eyewall shapes in Typhoon Wynne (1980). He made a fascinating analogy between polygonal eyewalls and the multiple vortices sometimes seen rotating around the inside of a parent tornado vortex, and noted barotropic instability as a possible cause of both phenomena. Kuo et al. (1999) and Reasor et al. (2000) documented elliptical eyewalls in Typhoon Herb (1996) and Hurricane Olivia (1994), respectively. Both studies noted elliptical eyewalls that rotated at approximately half the maximum tangential wind speed ( $V_{\max}$ ) with deep convection located at the ends of the major axis of the ellipse.

Other observational studies have confirmed the barotropic modeling results of Schubert et al. (1999) and Kossin and Schubert (2001) by documenting the existence of multiple mesovortices in the eye and substantial mixing between the eye and eyewall. Kossin et al. (2002, 2004) and Kossin and Schubert (2004) showed spectacular photographic and satellite imagery of low-level vortical swirls in the eyes of multiple Atlantic and Pacific basin tropical cyclones that closely resembled the long-lived mesovortices of Kossin and Schubert (2001). Using flight-level reconnaissance data, Kossin and Eastin (2001) showed that the radial profiles of vorticity and equivalent potential temperature ( $\Theta_e$ ) can undergo a rapid transition from a barotropically unstable regime with maximum values of vorticity and  $\Theta_e$  in the eyewall, to a stable regime with both maxima in the eye. Knaff et al. (2003) found that the development of annular hurricanes was systematically preceded by a dramatic asymmetric mixing event between the eye and the eyewall involving one or more mesovortices.

The most complete observational investigation of asymmetric vorticity dynamics and VRWs in the core of a tropical cyclone was carried out by Reasor et al. (2000) in Hurricane Olivia (1994). The vorticity asymmetry in the core was dominated by azimuthal wavenumber 2 below 3 km, and wavenumber 1 above 3 km, with maximum values of both found near the RMW. The wavenumber 1 signature was hypothesized to be the result of environmental vertical wind shear, as an increase in the magnitude of the wavenumber 1 asymmetry coincided with an increase in the magnitude of the vertical shear. The wavenumber 2 asymmetry was found to be the most unstable wavenumber and the natural by-product of the breakdown of the unstable vorticity ring that Olivia (1994) possessed at the beginning of the period of study. Reasor et al. (2000) also observed trailing bands of vorticity, 5–10 km wide, associated with high reflectivity, outside the eyewall of

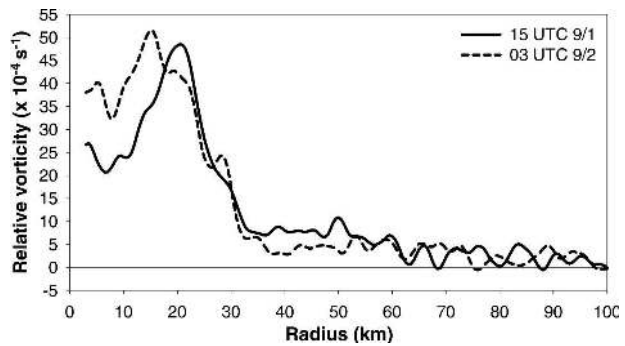


FIG. 1. Azimuthally averaged 850-hPa relative vorticity ( $\times 10^{-4} \text{ s}^{-1}$ ) at 1500 UTC 1 Sep (solid line) and 0300 UTC 2 Sep (dashed line). The averages were calculated over 4-h time periods centered on the time indicated.

Olivia (1994). They hypothesized that these bands were symmetrizing VRWs resulting from the expulsion of high-vorticity air from the core during mixing.

Motivated by the success of other observational studies in documenting VRWs in the core of tropical cyclones and the finding that the VRWs are well coupled to convection (Chen and Yau 2001; Reasor et al. 2000), in the present work an examination of the high spatial and temporal resolution radar dataset from Hurricane Elena (1985) was conducted to look for VRW activity. Figure 1 shows the 4-h azimuthal-mean 850-hPa vorticity profile centered on 1500 UTC 1 September calculated from National Oceanic and Atmospheric Administration (NOAA) reconnaissance flight data. As the storm rapidly intensified, Elena developed a ringlike vorticity profile similar to those shown to support barotropic instability by Schubert et al. (1999) and Reasor et al. (2000), with large radial gradients of vorticity on either side of the maximum. Figure 6 of Part I shows that undulations were seen along the inner edge of the eyewall, and reflectivity values above 15 dBZ appeared in the previously clear eye beginning around 1645 UTC. Each is suggestive of the presence of mesovortices and asymmetric mixing between the eye and eyewall. During this same time period, numerous high-reflectivity features were noted propagating outward from the deep eyewall convection (see Fig. 6 of Part I). A significant decrease in the number of outward-propagating features and a clearing of the eye began around 2130 UTC.

The WSR-57 data and fast Fourier transform used to decompose the reflectivity data into azimuthal wavenumber components are reviewed in section 2. Section 3 details the asymmetries in eyewall convection, including the appearance and rotation of an elliptical eyewall. The structure and propagation of four inner spiral rainbands with VRW characteristics are explored in section

4. Finally, a summary and discussion of the results is provided in section 5.

## 2. Data and methodology

### a. WSR-57 radar

Continuous radar scans of Elena's eyewall and inner rainbands were captured by Hurricane Research Division personnel with a portable data recorder attached to the WSR-57 at Apalachicola, Florida (AQQ), from 2200 UTC 31 August through 0200 UTC 2 September. A distance-dependent range correction that was constant beyond 230 km from the radar was applied to the raw-radar returned power (Burpee and Black 1989). During the time of this study (1310–2130 UTC 1 September), the center of Elena was within 120 km of the radar so that the inner 100 km of the storm was within 230 km of the radar at all times. The plots in this study will show full and decomposed reflectivity values beyond the 100-km radius, but caution must be used at these radii.

The reflectivity data were transformed from latitude–longitude coordinates to a storm-relative coordinate system with a domain of  $300 \text{ km} \times 300 \text{ km}$  and a horizontal resolution of 0.75 km (Burpee and Black 1989). Over 95% of the scans were made at an elevation angle of  $0.4^\circ$ . Alternate elevation angles (between  $0.5^\circ$  and  $0.9^\circ$ ) were eliminated from the dataset. Radar ground clutter was removed from each scan by manually setting all data points equal to zero within a rectangle centered on the radar site that encompassed the clutter. The box was then filled by bilinearly interpolating from the adjacent rows and columns of data.

Between 1300 and 2200 UTC 1 September, the AQQ radar made 313 scans of Elena, with as little as 23 s between complete radar scans. This short temporal resolution was possible due to Elena's close proximity to the radar, allowing a quarter to half a sweep of the radar to capture the reflectivity structure of Elena out to 150 km from the center. To have a uniform time step between radar images, the scans were linearly interpolated to 5-min intervals. Only the closest two scans to the time in question were weighted and used to compute the interpolated scan. If there were no scans within 5 min of either side of the prospective interpolated time, no scan was calculated and a gap appears in the data.

### b. Fast Fourier transform

Fourier analysis of the AQQ radar data was performed to separate the symmetric component of the reflectivity from higher-order azimuthal wavenumbers. The analysis was accomplished using FFTPACK from

the National Center for Atmospheric Research (Swarztrauber 1982) on the 5-min radar data that had been interpolated to a cylindrical grid with  $dr = 0.75 \text{ km}$  and  $d\lambda = 0.5^\circ$ . In the case of Elena, azimuthal wavenumbers 1–360 were possible as there were 720 points around in azimuth, but very little power (defined as wave amplitude squared) existed in wavenumbers greater than 2 (Corbosiero 2005).

Fourier analysis of radar reflectivity is not the best way to isolate wave activity. Only convectively coupled VRWs can be captured by analysis of the radar data. Three-dimensional wind and stability analyses would be needed to calculate PV. Nevertheless, reflectivity is proportional to a physical quantity, the rainfall rate. Most importantly, only radar reflectivity is available with such high temporal and spatial resolution.

Reasor et al. (2000) noted that the magnitude of wavenumber 1 is sensitive to the definition of the vortex center, while wavenumber 2 is fairly robust. In the case of Elena, the center of the cylindrical grid from which the FFT was calculated was the *dynamical* center of the vortex determined by the Willoughby and Chel-mow (1982) method, and not the *geometrical* center of the clear eye as seen in the individual radar scans. Thus, two possible sources of erroneous wavenumber 1 amplitude exist: 1) small time-scale fluctuations in track not captured by the series of cubic splines used to determine the track (Willoughby and Chel-mow 1982) and 2) the changing eye and eyewall shapes such that the dynamical center and geometrical center of the eye are not coincident. In recognition of these possible sources of error, the time variations of the amplitude in wavenumber 1 will not be discussed in detail.

## 3. Structure of the eyewall convection

### a. Wavenumbers 0 and 1

Figure 2 shows the power for azimuthal wavenumbers 0, 1, and 2 from 1310 to 2130 UTC 1 September. Values are averaged over the radial band 20–30 km from the center of Elena, encompassing the mean position of the eyewall. From Fig. 2 it is clear that wavenumber 0, the symmetric reflectivity structure, dominated the eyewall reflectivity pattern at all times by at least a factor of 2 (note the break in the vertical axis scale). Figure 3 shows the azimuthal distribution of wavenumber 1 averaged over the same radial band as Fig. 2. The wavenumber 1 azimuthal maximum remained north to northwest of the center throughout the period. During this same period, the environmental vertical wind shear (see Table 1 in Part I) was from the northwest between 6 and  $9 \text{ m s}^{-1}$ . The wavenumber 1 pattern shown in Fig. 3 fits the shear-induced reflectiv-

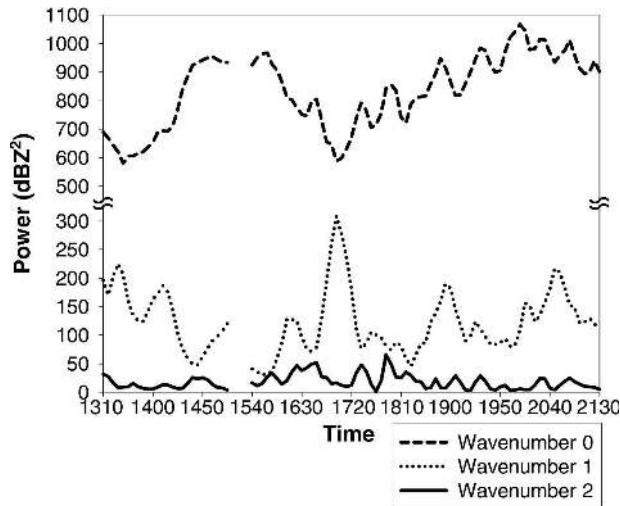


FIG. 2. Power in wavenumbers 0–2 averaged over the radial range of 20–30 km from the center of Elena from 1310 to 2130 UTC 1 Sep.

ity pattern with high reflectivity extending from the left of shear to upshear, consistent with both numerical models (Braun 2002; Rogers et al. 2003) and observations (Willoughby et al. 1984; Franklin et al. 1993; Black et al. 2002) of tropical cyclones.

The variation of the power in wavenumber 0 in Fig. 2 was broadly anticorrelated with that in wavenumber 1, with a correlation coefficient of  $-0.44$ . This indicates an amplitude fluctuation between the symmetric component and the shear-induced wavenumber 1 asymmetry, consistent with theory and observations (Jones 1995; Reasor et al. 2000). The strength of the anticorrelation, however, varied significantly with time. During the period of 1400–1555 UTC 1 September, when the dynamic and geometric centers discussed above were nearly coincident, the correlation coefficient was  $-0.85$ . For the period 1900–2055 UTC, when the centers were farther apart, the correlation was  $0.005$ . These results suggest that when the difference between the dynamic and geometric centers is large, an additional, erroneous wavenumber 1 asymmetry is introduced, as discussed in the last section. This masks the otherwise strong anticorrelation and interplay between the symmetric and shear-induced storm structures.

#### b. Wavenumber 2 and evolution of the elliptical eyewall

As will be seen in figures in this and the next section, Elena's eyewall exhibited many noncircular shapes including ellipses (Fig. 4a), triangles (Fig. 7e), and squares (Fig. 9a). Most of these features were short lived, with the exception of an elliptical eyewall that was traceable for over 2 h (1450–1700 UTC 1 Septem-

ber) as its major axis completed one full rotation. Figure 4 details half of the rotation cycle of the ellipse, showing AQQ radar scans every 10 min from 1545 to 1645 UTC 1 September. The images have been blown up to only show the eye and eyewall, with the inner and outer circles representing the 30- and 50-km radii, respectively. Previous authors have shown elliptical eyewalls to be associated with wavenumber 2 asymmetries (e.g., Kuo et al. 1999). The dashed lines in the images of Fig. 4 connect the positive anomalies in wavenumber 2 at the 30-km radius shown in Fig. 5.

At 1545 UTC (Fig. 4a), the elliptical eyewall of Elena was oriented approximately north–south with deep convection located at the ends of the major ellipse axis. The eyewall also exhibited strong power in wavenumber 1 due to forcing from vertical wind shear with maximum values north of the center, or left of shear, as shown in Fig. 3. At this time a low-reflectivity region was located just outside the 30-km radius northwest of the center. This low-reflectivity region grew in scale and rotated cyclonically around the center at approximately the same speed as the elliptical eyewall (Figs. 4b and 4c). By 1615 UTC (Fig. 4d) the eyewall had taken on an approximate east–west orientation.

Between 1625 and 1645 UTC 1 September (Figs. 4e–g) the elliptical eyewall rotated back to a north–south orientation, and the once-clear eye became filled with low-level clouds and reflectivities between 4 and 16 dBZ. Another dramatic structural change was the erosion of the southwestern eyewall due to the intrusion of the rotating region of low reflectivity. Indeed, it was the growth of this feature that produced the large increase in the wavenumber 1 asymmetry seen in Figs. 2 and 3 beginning around 1645 UTC. This effect can be seen by comparing the reflectivity between the two radii circles in Figs. 4a and 4g. In just 1 h, all traces of deep convection were eroded southwest of the center, while almost the entire northeastern quadrant had radar reflectivities greater than 32 dBZ, setting up the strong wavenumber 1 asymmetry.

A similar sequence of events was seen in IR satellite images by Knaff et al. (2003) in Hurricane Luis (1995). Shown in their Fig. 5, a warm cloud-top region rotated around the storm and appeared to cause the breakdown of the eyewall. They hypothesized that this warm cloud-top region was associated with a mesovortex seen rotating on the inner edge of the eyewall as an undulation in the eyewall clouds. Coincident with the eyewall breakdown (their Fig. 5e) was the appearance of an elliptical eyewall and nonzero reflectivity in the previously clear eye due to the mixing effects of the mesovortices. Supporting this idea of eyewall breakdown, Knaff et al. (2003) found that prior to the mixing event

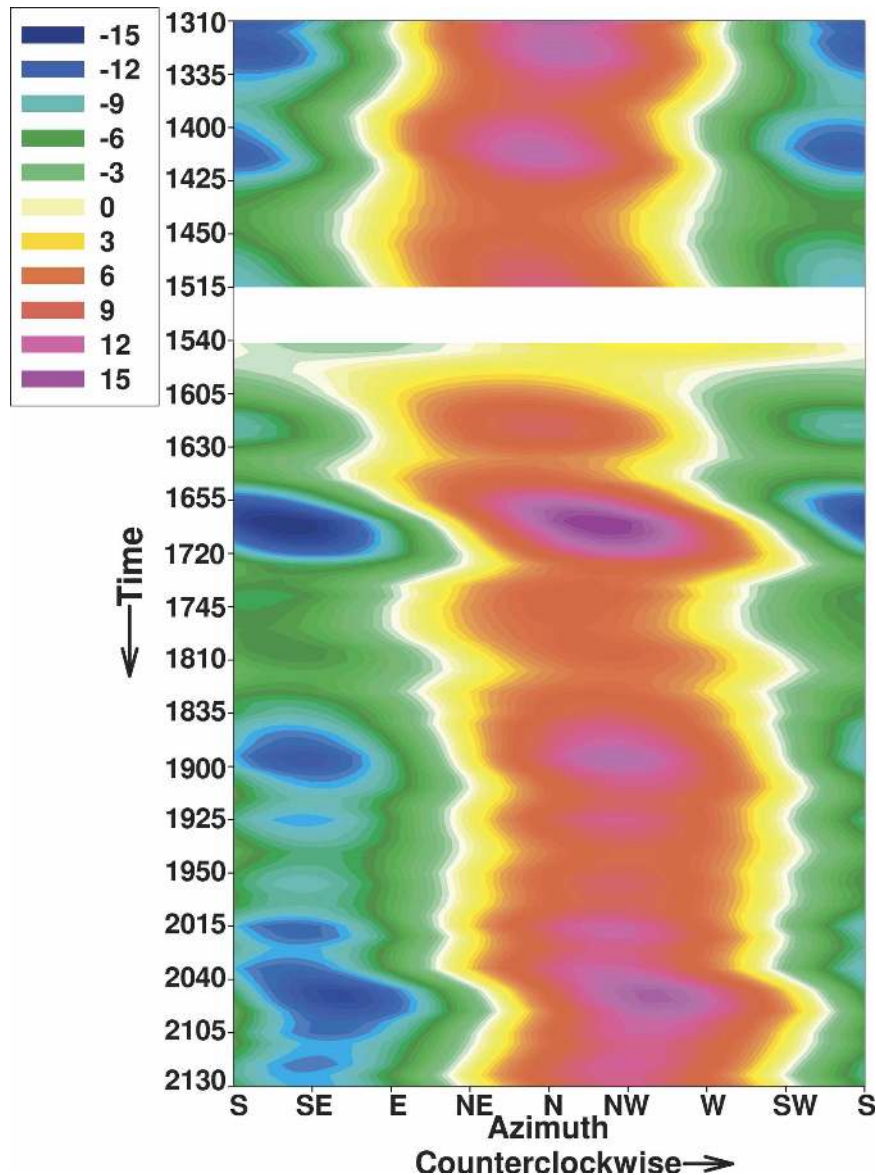


FIG. 3. Azimuth-time Hovmöller diagram of the wavenumber 1 asymmetry averaged 20–30 km from the center of Elena. The white strip represents a gap in the Apalachicola, FL, radar data.

the radial profile of vorticity in Hurricane Luis (1995) satisfied the Rayleigh necessary condition for barotropic instability.

In Elena, a strong vorticity maximum of nearly  $50 \times 10^{-4} \text{ s}^{-1}$  had developed on the inner edge of the eyewall ( $\sim 20$  km from the center) with much lower values on either side by 1500 UTC 1 September (Fig. 1). The radial vorticity structure at this time was strikingly similar to the profile found by Reasor et al. (2000) in Hurricane Olivia (1994) to be most unstable to wavenumber 2 asymmetries (their Figs. 11b and 17). The appearance of an elliptical eyewall and increase in the

magnitude of wavenumber 2 in Elena is thus hypothesized to result from the growth of unstable VRWs propagating within the eyewall and the pooling of vorticity into mesovortices in the eye as detailed by Schubert et al. (1999), Kossin and Schubert (2001), and Knaff et al. (2003).

Lending further support to the existence of mesovortices in Elena are the concurrent clearing of the eye and decrease in outward-propagating features around 2200 UTC 1 September seen in Fig. 6 of Part I. Knaff et al. (2003) documented the same result and hypothesized that mesovortices within the eye effectively mixed high

PV from the eyewall into the eye, stabilizing the vorticity profile and leading to the cessation of the outward-directed PV ejection that must accompany these mixing events (Guinn and Schubert 1993; Schubert et al. 1999). After the appearance of the elliptical eyewall (Fig. 1), the vorticity profile did not completely relax to a monopole as was noted in Knaff et al. (2003) and Kossin and Eastin (2001). The peak vorticity actually increased slightly from its value 12 h earlier due to the continued diabatic generation of vorticity in the eyewall. Nevertheless, Fig. 1 shows that by 0300 UTC 2 September, vorticity inside the eye had increased significantly to  $\sim 40 \times 10^{-4} \text{ s}^{-1}$  as the width of the vorticity peak broadened and the gradients on either side of the peak weakened. Although the radar data do not allow for the direct observation of mesovortices, the results above suggest that they existed and produced significant mixing between the eye and eyewall.

Figure 5 shows an azimuth–time diagram of the wavenumber 2 asymmetry at the 30-km radius. The positive wavenumber 2 asymmetry completed one full rotation at a tangential speed of  $27 \text{ m s}^{-1}$  between 1445 and 1640 UTC. The maximum tangential wind speed from the NOAA WP-3 aircraft at 850 hPa at this time was  $51 \text{ m s}^{-1}$ , so that the ellipse rotated at  $\sim 53\%$  of  $V_{\text{max}}$ . These speeds are consistent with the elliptical eyewall and wavenumber 2 asymmetry rotation rates of  $\sim V_{\text{max}}/2$  found by Kuo et al. (1999) and Reasor et al. (2000). These azimuthal phase speeds are also consistent with the speed of a linear PV wave propagating on the vorticity discontinuity in a Rankine vortex given by  $C_\lambda = V_{\text{max}}(1-1/n)$ , where  $n$  is the azimuthal wavenumber of the asymmetry (Lamb 1932).

In addition to the eyewall features noted above, two bands of high reflectivity broke off of the deep convection in the northern eyewall between 1545 and 1645 UTC 1 September (Figs. 4c, 4f, and 4g). These features continued to propagate cyclonically and radially outward from the eyewall, moving past the 50-km radius and off the image into the northwest quadrant. As will be seen in the next section, these features propagated outward and manifested themselves as inner spiral rainbands with VRW characteristics as discussed by Montgomery and Kallenbach (1997) and Chen et al. (2003).

#### 4. Structure of convection outside the eyewall

Figure 6 shows the time series of the power of azimuthal wavenumbers 0–2 averaged 55–90 km from the center of Elena. This radial range was chosen to fall outside the eyewall and to encompass the typical region of the inner, or secondary, spiral rainbands (Willoughby et al. 1984). Similar to the power in the eyewall region shown in Fig. 2, the inner rainband region re-

flectivity structure was dominated by a slowly varying contribution from wavenumber 0, while wavenumbers 1 and 2 contained much lower power. The amplitudes of both wavenumbers 0 and 1 were significantly smaller than their values in the eyewall, with the average power in wavenumber 0 reduced by a third and wavenumber 1 cut by half. The inner rainband region otherwise differed from the storm core in that wavenumber 2 was frequently close to, and for a short time exceeded, the power in wavenumber 1.

Figure 6 shows that the evolution of the power in wavenumber 2 contained four peaks seen at  $\sim 1430$ , 1635, 1850, and 2000 UTC 1 September. These four peaks are explored below and each is found to be associated with an inner spiral rainband in the raw reflectivity field. In the discussion of these bands, the term *rainband* or *band* will be used to describe a distinct convective feature in the raw reflectivity field that takes the form of a trailing spiral with regions of much lower reflectivity on either side.

Figure 7 details the appearance, growth, and decay of the second of these bands. As the rainband shown in the raw reflectivity field (left panels in Fig. 7) possessed a strong wavenumber 2 component, it is thus associated with two maxima and two minima in the wavenumber 2 asymmetry shown on the right. The AQQ radar scans show the full 150 km from the center with the inner circle representing the 50-km radius. The location of the AQQ radar can be seen as the crescent-shaped region of reflectivity exceeding 36 dBZ about 110 km north-northwest of the center of Elena.

At 1600 UTC (Fig. 7a), the developing rainband was seen curving outward from 50 km south of the center to 60 km west of the center in the 32-dBZ contour. The band was just beginning to exhibit a weak wavenumber 2 amplitude of less than 6 dBZ  $\sim 50$  km southwest of the center. The strongest wavenumber 2 asymmetry at this time was located inside the 50-km radius in association with the elliptical eyewall discussed earlier. Active convection in the eyewall was oriented approximately northwest–southeast in Fig. 7a, consistent with Fig. 4b at nearly the same time. During the next 20 min, deep convection intensified along the band so that by 1620 UTC (Fig. 7b), the feature was fully formed and spanned the entire southwestern quadrant of the storm with an amplitude in wavenumber 2 approaching 12 dBZ. As noted earlier, the rainband to the southwest of the center represents just one-quarter of the wavenumber 2 feature. Although somewhat obscured by the strong wavenumber 1 signal induced by the environmental vertical wind shear (Fig. 3), the other positive reflectivity anomaly of the VRW can be seen as the band of reflectivity  $>36$  dBZ spiraling outward from

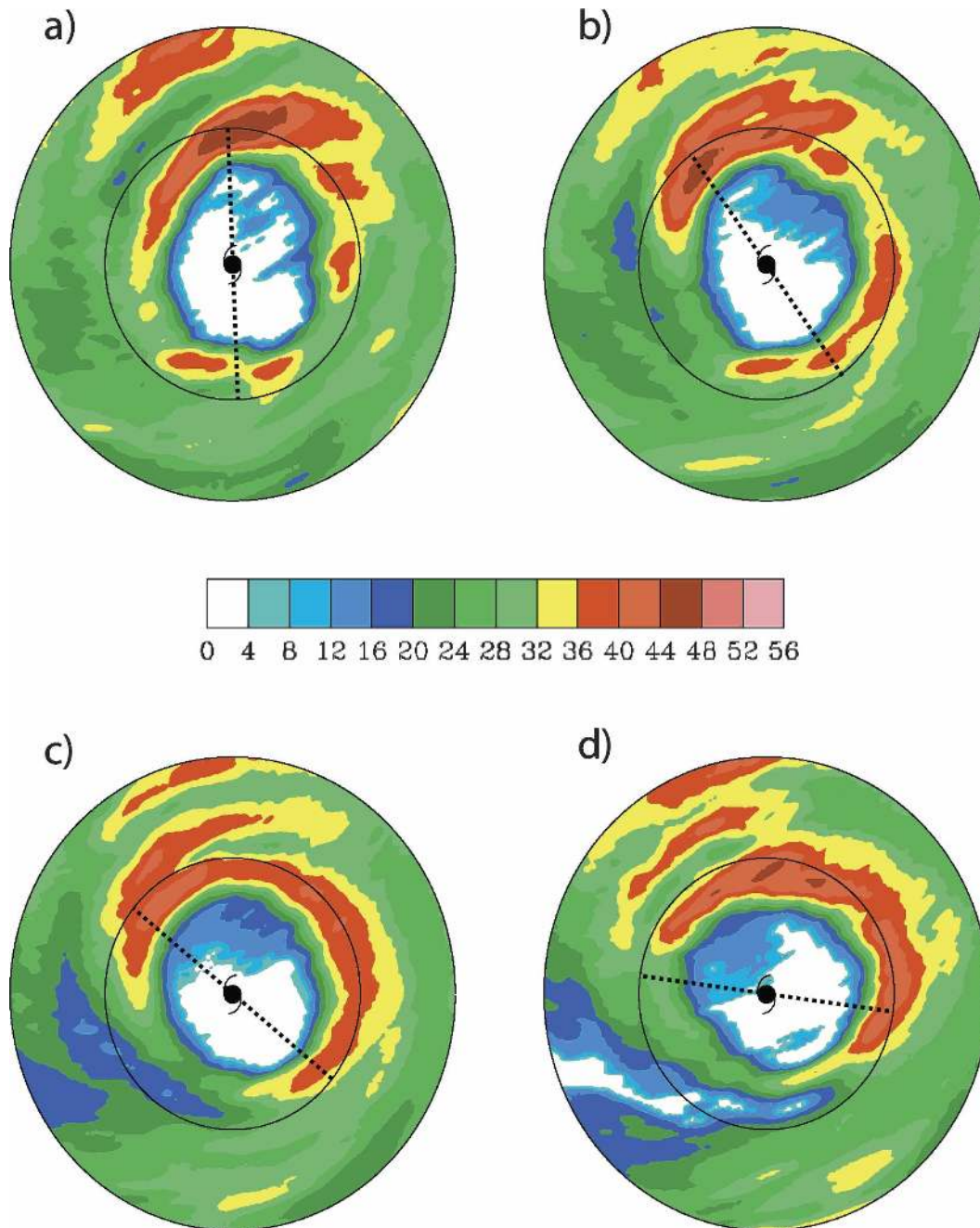


FIG. 4. Apalachicola, FL, radar scans of Elena at (a) 1545, (b) 1555, (c) 1605, (d) 1615, (e) 1625, (f) 1635, and (g) 1645 UTC 1 Sep. The inner and outer circles are the 30- and 50-km radii, respectively. The dashed line connects the positive wavenumber 2 anomalies at 30 km shown in Fig. 5.

the 50-km radius northwest of the center to 60 km east-northeast of the center.

Between 1600 and 1640 UTC (Figs. 7a and 7c), the low-reflectivity region discussed in the last section rotated around the center and expanded in areal coverage, in concert with the invigoration of convection along the band and the growth in wavenumber 2. Dur-

ing this period, the cyclonic rotation of the elliptical eyewall (Figs. 4c–e and 7b) brought it into an orientation where the wavenumber 2 asymmetries associated with the eyewall and the band were in phase, located at the 25- and 50-km radii, respectively. The average relative vorticity profile at 850 hPa during this period (Fig. 8) shows that these two wavenumber 2 features were

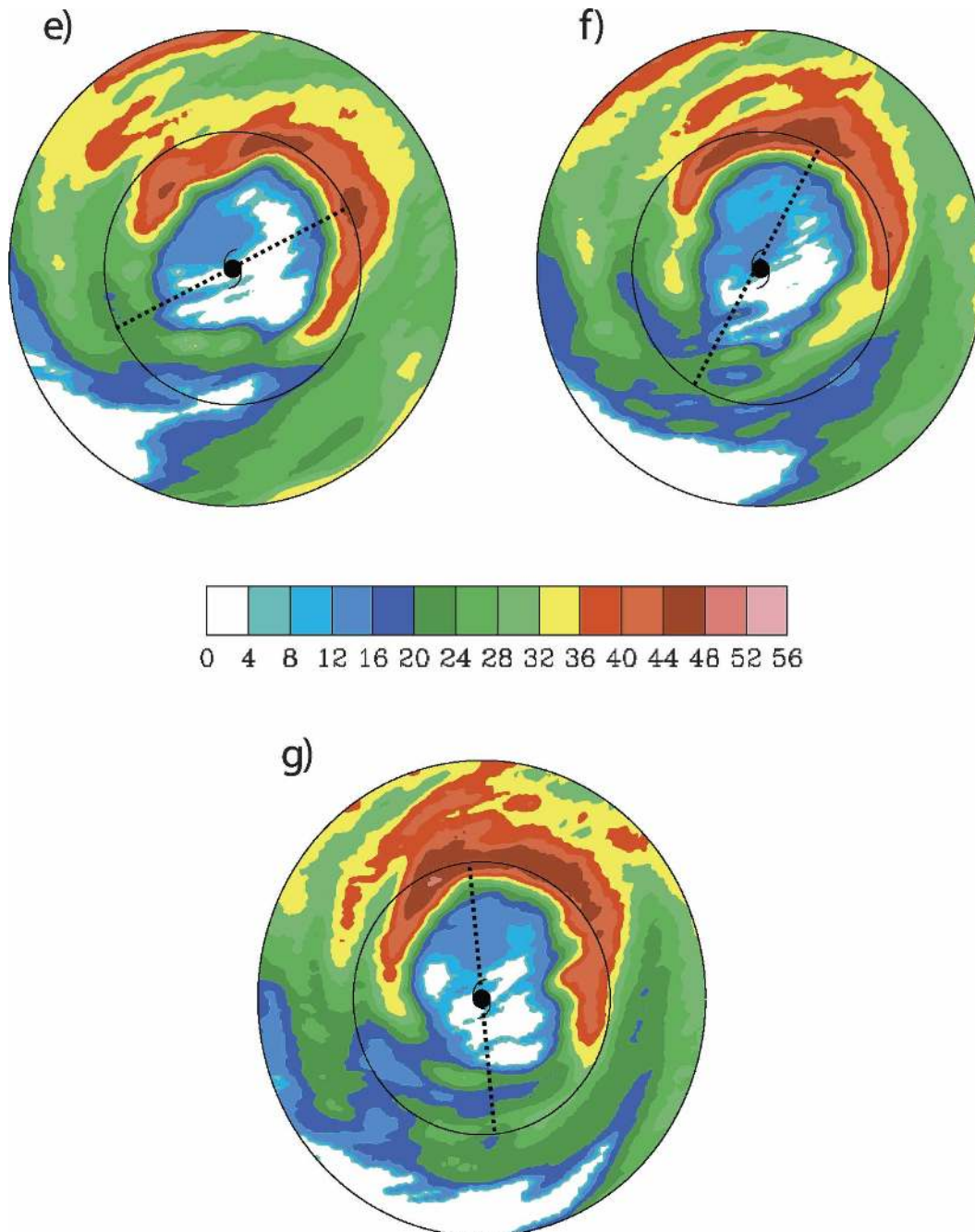


FIG. 4. (Continued)

located on strong, opposite-signed, radial gradients of vorticity. The inner feature was propagating along the negative radial gradient of the eyewall vorticity, while the outer wavenumber 2 feature was associated with a positive radial gradient of vorticity located inside a secondary, outer ring of vorticity. Located between the two vorticity peaks was a moat of low vorticity (located at the 35–48-km radii in Fig. 8).

As first discussed by Kossin et al. (2000), because the

radial gradient of vorticity changes sign across the low-vorticity moat, unstable interactions may occur between the counterpropagating VRWs located on the two, oppositely signed vorticity gradients if the moat is sufficiently narrow. The Elena vorticity profile shown in Fig. 8 is quite similar to the type II instability profile in Kossin et al. (2000) (their Fig. 12) with respect to the width of the moat (10–12 km), distance between vorticity maxima (20–30 km), and relative strengths of the

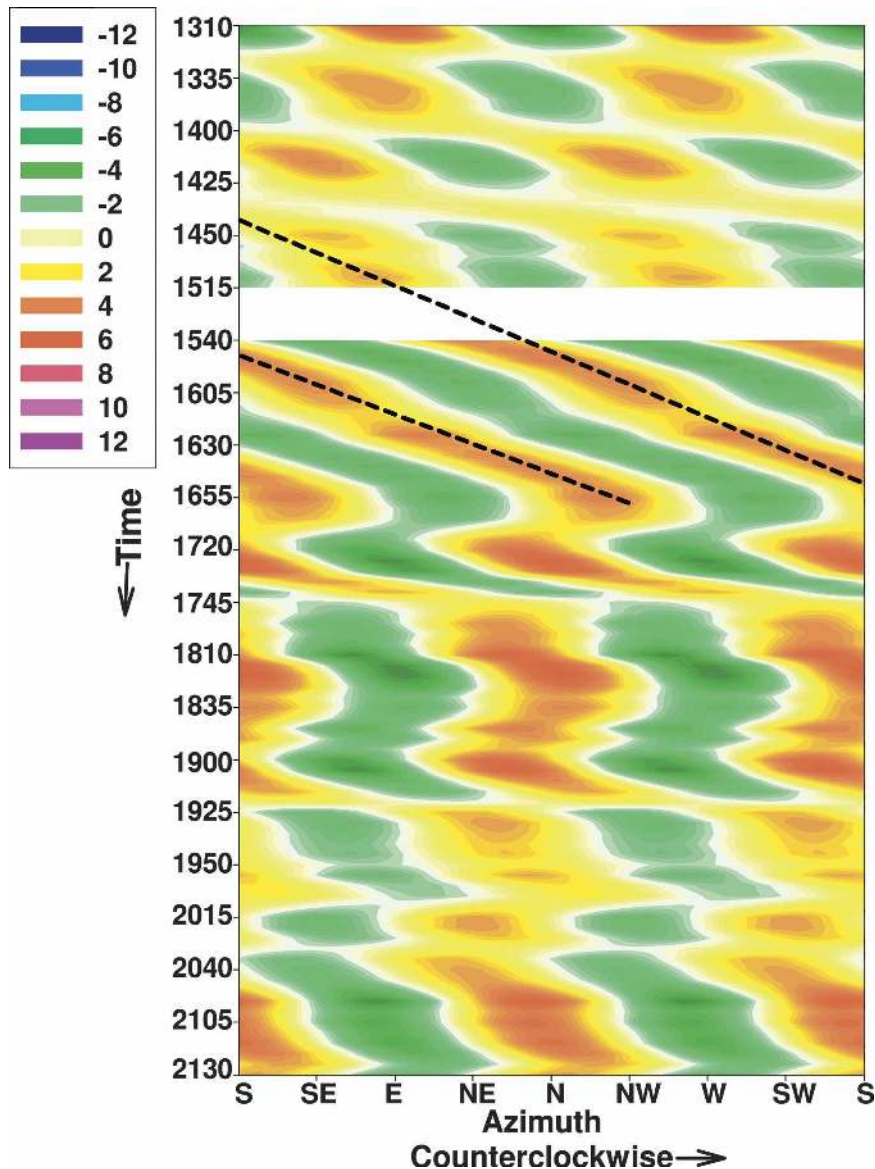


FIG. 5. Azimuth-time Hovmöller diagram of the wavenumber 2 asymmetry at 30 km from the center of Elena. The dashed line follows the positive wavenumber 2 reflectivity anomaly and the rotation of the elliptical eye.

maxima (ratio of eyewall to outer peak of 5:1). Further supporting the idea of instability across the moat is that the power in wavenumber 2 in the eyewall (Fig. 2) and rainband regions (Fig. 6) both increased during this period and the two wavenumber 2 asymmetries were radially aligned (Fig. 7b), suggesting a phase locking and mutual growth of these features.

Outside of the convection in the eyewall, the dominant reflectivity features in Elena at 1640 UTC (Fig. 7c) were the rainband southwest of the center with reflectivities exceeding 40 dBZ along its length and the large area of reflectivity >32 dBZ north and northeast of the

center. The band spiraled anticyclonically outward from 50 km southeast of the center to 90 km west of the center. The convectively suppressed part of the wave had nearly zero reflectivity southwest of the center, but was masked by the vertical wind shear signal in the northeast, or downshear-left, quadrant. The cyclonic and outward propagation of the band can be seen by comparing Figs. 7a and 7c. The inner tip of the band rotated  $\sim 45^\circ$  from south-southwest to south-southeast of the center, while the far end moved outward from the 60–80-km radii.

Between 1700 and 1720 UTC (Figs. 7d and 7e), the

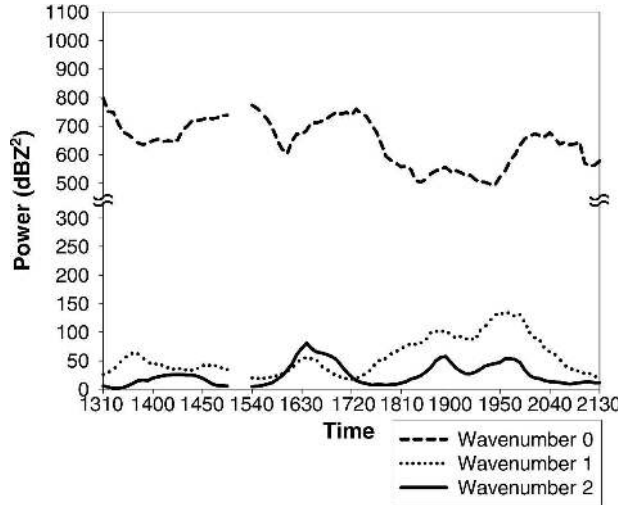


FIG. 6. Power in wavenumbers 0–2 averaged over the radial range of 55–90 km from the center of Elena from 1310 to 2130 UTC 1 Sep.

band propagated slowly outward and cyclonically around the center and began to noticeably thin and lose its deep convection and wavenumber 2 signal. The wavenumber 2 amplitude in the eyewall was also decreasing at this time as the elliptical eyewall appeared to have “outrun” the inner rainband. The eyewall was also noted to be losing its elliptical shape and transitioning to a nearly stationary wavenumber 2 pattern that persisted for the rest of the time period of study (Fig. 5). At 1720 UTC, as the band reached the 90-km radius, it appeared to break into two pieces that continued to be stretched and thinned by the shear of the angular velocity, so that by 1740 UTC (Fig. 7f) little evidence of the band remained in the full reflectivity or wavenumber 2 fields. However, the feature that would become the last rainband and significant peak in wavenumber 2 power had already formed, and was located  $\sim 35$  km west-northwest of the eye, curving outward to the 50-km radius north of the center in Fig. 7f. This rainband originated from the bump in the 40-dBZ contour just beginning to separate from the main eyewall north-northwest of the center at 1720 UTC (Fig. 7e). This evolution is similar to the banded features that were noted to break off from the eyewall convection in Figs. 4c and 4g.

Figure 9 shows images of the full radar reflectivity (left panels) and wavenumber 2 asymmetry (right panels) near the times of each of the other peaks in wavenumber 2 (Fig. 6). At peak intensity, all bands possessed reflectivities greater than 40 dBZ located along a band south of the center near the 55-km radius, with much lower values on either side. The positive reflec-

tivity anomalies in wavenumber 2 were always located southwest and northeast of the center for each of the four cases (right panels in Figs. 7 and 9). Each of the bands appeared to have a similar origin, breaking off of and propagating away from the deep convection in the northern eyewall. As will be seen below, they also have similar cyclonic and outward propagation speeds.

Because the bands possessed significant power in wavenumber 2, the azimuthal phase speeds of the bands were determined from an azimuth–time Hovmöller diagram of the wavenumber 2 asymmetry at the 80-km radius shown in Fig. 10. Four cyclonically rotating wavenumber 2 features of  $>6$  dBZ are evident, corresponding to the four peaks in wavenumber 2 power in Fig. 6. Each was associated with an inner spiral rainband as shown in Figs. 7 and 9. The bands in Fig. 10 repeatedly appeared at the 80-km radius west of the center and rotated cyclonically through  $\sim 90^\circ$  of azimuth before moving radially outward past the 80-km radius. The black solid lines in the figure follow the azimuthal rotation of the bands. They were used to calculate azimuthal phase speeds of 24, 23, 20, and 31  $\text{m s}^{-1}$ , respectively, for the bands from top to bottom.

The bands were moving more slowly than the local tangential wind, at approximately 73%, 64%, 53%, and 80% of the wind speed, respectively. These percentages are much larger than the 50% of the tangential wind obtained from the formula for the speed of a wavenumber 2 PV edge wave in a Rankine vortex given in the last section. Elena, however, like most hurricane-strength vortices (Mallen et al. 2005), was not Rankine (i.e., the vorticity gradient is not confined to a single radius; see Fig. 1). In recognition of this fact, Montgomery and Kallenbach (1997) and Möller and Montgomery (2000) derived a dispersion relationship for baroclinic disturbances propagating on a barotropic circular vortex in gradient and hydrostatic balance:

$$\omega = n\bar{\Omega} + \frac{n}{R} \frac{\bar{\xi}}{\bar{q}} \frac{\frac{\partial \bar{q}}{\partial r}}{[k^2 + n^2/R^2 + (\bar{\eta}\bar{\xi}m^2)/N^2]}, \quad (1)$$

where  $n$ ,  $k$ , and  $m$  are the azimuthal, radial, and vertical wavenumbers, respectively; the overbar denotes the azimuthal mean or basic state;  $R$  is the reference radius (Reasor et al. 2000);  $(\partial \bar{q}/\partial r)$  is the radial derivative of the barotropic basic-state PV;  $\bar{\eta}$  is the absolute vorticity;  $\bar{\xi}$  is the inertia parameter;  $N^2$  is the static stability; and  $\bar{\Omega}$  is the angular velocity. From this formula, the radial change of the azimuthal phase speed of the wave ( $C_\lambda = \omega R/n$ ) is found to depend most heavily on two variables: 1) the radial gradient of PV,  $(\partial \bar{q}/\partial r)$ , which decreases sharply outside the 35-km radius (Fig. 1), and

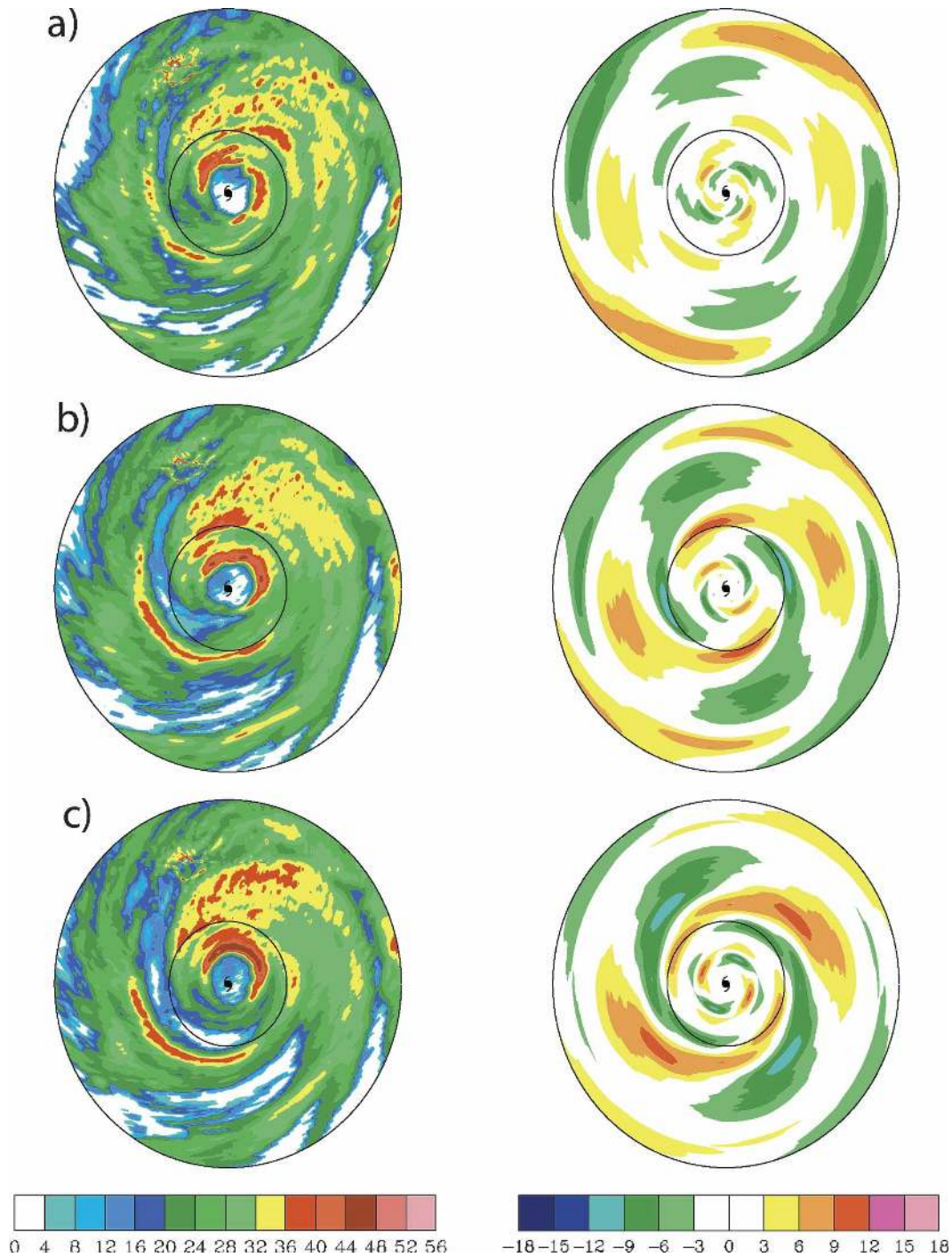


FIG. 7. Apalachicola (left) radar reflectivity and (right) wavenumber 2 asymmetry of Elena at (a) 1600, (b) 1620, (c) 1640, (d) 1700, (e) 1720, and (f) 1740 UTC 1 Sep. The inner and outer circles are the 50- and 150-km radii, respectively.

2) the radial wavenumber,  $k$ , which increases as the waves move outward due to strong horizontal shearing. As convectively active bands propagate outward and away from the eyewall, these two quantities will act to

reduce the magnitude of the second term on the right-hand side of Eq. (1), reducing the retrograde speed of the wave; that is, the band will propagate at a higher fraction of the mean cyclonic wind.

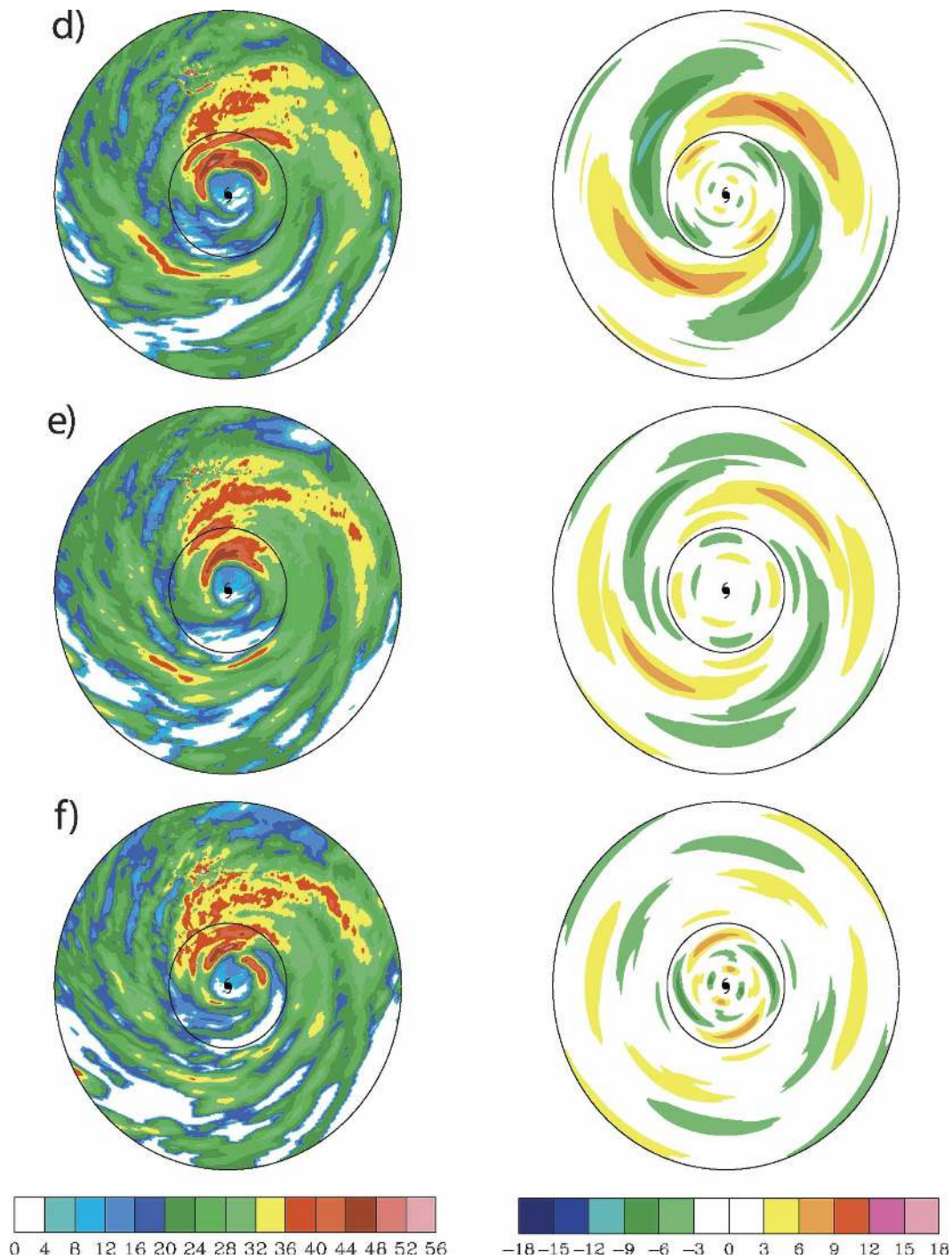


FIG. 7. (Continued)

Using the Fourier decomposed radar reflectivity and reconnaissance flight data collected in Elena, it was possible to estimate all of the quantities needed to calculate the azimuthal phase speed from Eq. (1), except for the static stability ( $N^2$ ) and the vertical wavenumber ( $m$ ). Values for these quantities were estimated

from the modeling studies of Chen and Yau (2001) and Wang (2002a) who documented propagating rainbands very similar to those observed in Elena. Taking  $N^2 = 1.5 \times 10^{-4} \text{ s}^{-1}$  and  $m = 2\pi/L = 4.2 \times 10^{-4} \text{ m}^{-1}$ , and evaluating all other quantities at the reference radius,  $R = 80 \text{ km}$ , during the time of the second major band

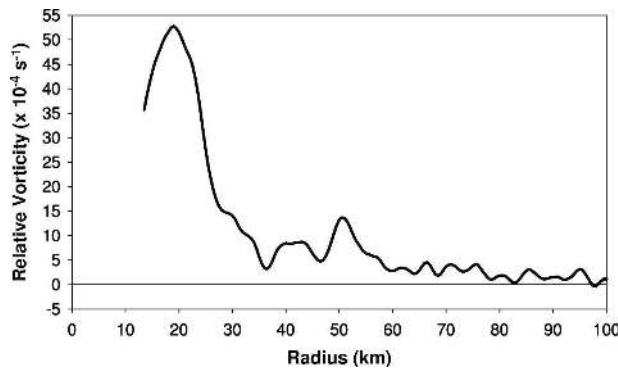


FIG. 8. Average 850-hPa relative vorticity ( $\times 10^{-4} \text{ s}^{-1}$ ) between 1450 and 1730 UTC 1 Sep.

(Fig. 7),  $V_t = 36 \text{ m s}^{-1}$ ,  $\bar{\Omega} = 4.5 \times 10^{-4} \text{ s}^{-1}$ ,  $\bar{\xi} = 9.7 \times 10^{-4} \text{ s}^{-1}$ ,  $n = 2$ ,  $k = 2\pi/L = 9 \times 10^{-5} \text{ m}^{-1}$ ,  $\bar{\eta} = 2.7 \times 10^{-4} \text{ s}^{-1}$ , and  $(\partial\bar{\eta}/\partial r) = 2.5 \times 10^{-8} \text{ m}^{-1} \text{ s}^{-1}$ . As it was not possible to calculate PV ( $q$ ) from the available data in Elena, horizontal variations in stability were neglected and it was assumed that  $(1/\bar{q})(\partial\bar{q}/\partial r) \approx (1/\bar{\eta})(\partial\bar{\eta}/\partial r)$ . Using all of these values in evaluating the azimuthal phase speed,  $C_\lambda = \omega R/n$ , gives a value of  $26 \text{ m s}^{-1}$ , nearly equivalent to the  $23 \text{ m s}^{-1}$  deduced from Fig. 10.

The azimuthal phase speeds determined from Fig. 10 are also consistent with the VRW speeds of Chen and Yau (2001) and Wang (2002a). The Elena band speeds of between 50% and 80% of the tangential wind are similar to the 60%–80% of  $V_{\text{max}}$  found by Black et al. (2002) for convective cells in east Pacific Hurricanes Jimena (1991) and Olivia (1994) and the observation by Senn and Hiser (1959) that hurricane rainbands rotated cyclonically around the center more slowly than the local tangential wind. To date, however, there exist no other observational studies of inner-rainband azimuthal speed to compare to the phase speeds found here.

Figure 11 shows a radius–time Hovmöller diagram of the wavenumber 2 reflectivity along an azimuth drawn from the center of Elena out toward the southwest, the most active quadrant for rainband activity. Again, four distinct outward-propagating wavenumber 2 features are evident. They repeatedly appeared in the southwest quadrant near the 50-km radius and propagated outward to between the 90- and 100-km radii with an average speed of  $5.2 \text{ m s}^{-1}$ .

The VRW radial phase speed from Möller and Montgomery (2000) is  $C_r = \omega/k$ . Using the quantities defined above for the second rainband at 1700 UTC 1 September and  $R = 80 \text{ km}$ , the radial phase speed of a wavenumber 2 VRW should be outward at  $7.2 \text{ m s}^{-1}$ . This value is similar to the  $5.4 \text{ m s}^{-1}$  for the second rainband at the 80-km radius determined from Fig. 11. Thus, both

the radial and azimuthal phase speeds of the wavenumber 2 bands observed in Elena are consistent with VRW theory. Although the close agreement might be serendipitous given the uncertainty in some of the input values, it suggests the identification of the features as VRWs is reasonable.

As was seen in Figs. 7 and 9, the four spiral bands studied here began to thin at around the 80-km radius and did not propagate much past 100 km from the center. This effect can also be seen in Fig. 11, as the outward phase propagation (shown by solid curves) of the wavenumber 2 features ceased around the 100-km radius. The outward *group* propagation (seen by following the maxima and minima in wavenumber 2 forward in time), however, ceased closer to the center, around the 90-km radius (vertical dashed line in Fig. 11). Montgomery and Kallenbach (1997) noted that as VRWs propagate outward, they are continually thinned by the shear of the angular velocity, increasing their radial wavenumber ( $k$ ) and slowing their outward propagation. The radial phase speed is  $\sim O(k^{-1})$ , while the radial group velocity is  $\sim O(k^{-3})$ . In theory, the outward group velocity should thus cease before the phase velocity, just as is seen in Fig. 11.

In the simulations of Montgomery and Kallenbach (1997), the shearing effect of the angular velocity became dominant as time progressed, and the outward group propagation of the waves ceased at the stagnation radius, located at  $r \approx 3 \times \text{RMW}$  (Tuttle and Gall 1995; Montgomery and Kallenbach 1997). The average RMW during the time period of rainband activity in Elena was  $\sim 30 \text{ km}$ , placing the stagnation radius of Montgomery and Kallenbach (1997) at the 90-km radius, consistent with the cessation of outward group propagation seen in Fig. 11.

## 5. Summary and discussion

In Part I of this paper, Corbosiero et al. (2005) showed that the spinup of the tangential wind and increase in deep convection within the eyewall of Hurricane Elena (1985) acted to increase the vorticity maximum on the inner edge of the eyewall between 1100 and 1500 UTC 1 September. The 850-hPa eyewall vorticity maximum was surrounded by much lower values on either side, producing an annular vorticity profile, similar to those shown in observations (Reasor et al. 2000) and numerical models (Schubert et al. 1999) to support barotropic instability. Between 1500 and 1700 UTC 1 September, the eyewall took on an elliptical shape that rotated with the speed of a wavenumber 2 PV edge wave (Figs. 4 and 5). The previously clear eye was also noted to fill with low-level clouds. Twelve

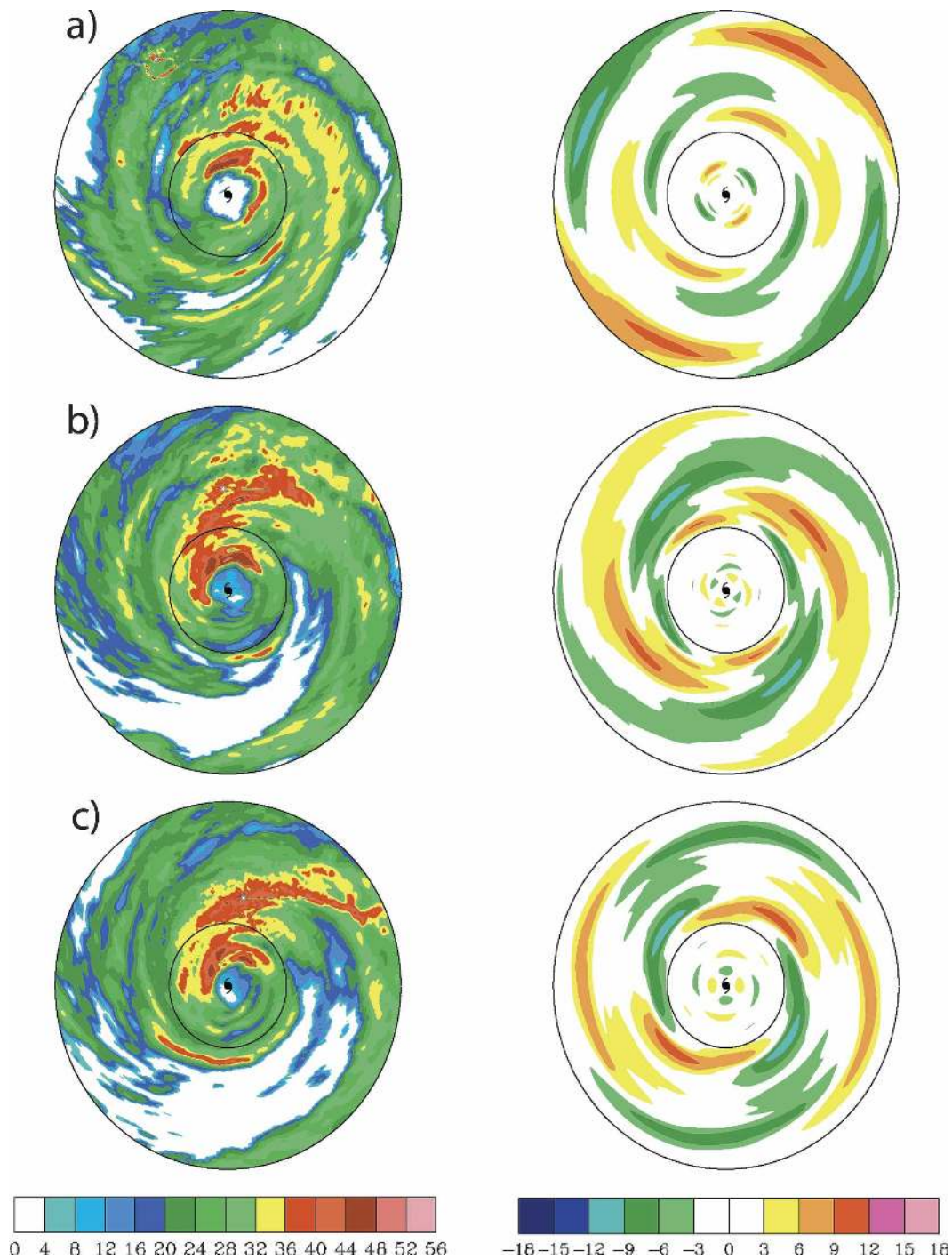


FIG. 9. As in Fig. 7 but for three additional rainbands at (a) 1440, (b) 1850, and (c) 1955 UTC 1 Sep.

hours later, the low-level vorticity profile had broadened and values had nearly doubled within the eye (Fig. 1).

The sequence of events described above is consistent with the realization of barotropic instability within the eyewall, the breakdown of eyewall vorticity into mesovortices, and asymmetric mixing between the eye and

eyewall. Previous studies have suggested that such a mixing event may act as a natural break on the rapid intensification of tropical cyclones, as the asymmetric mixing was noted to cause an increase in the tangential winds in the eye, and a decrease at the RMW (Kossin and Schubert 2001; Chen and Yau 2003). In Elena, the

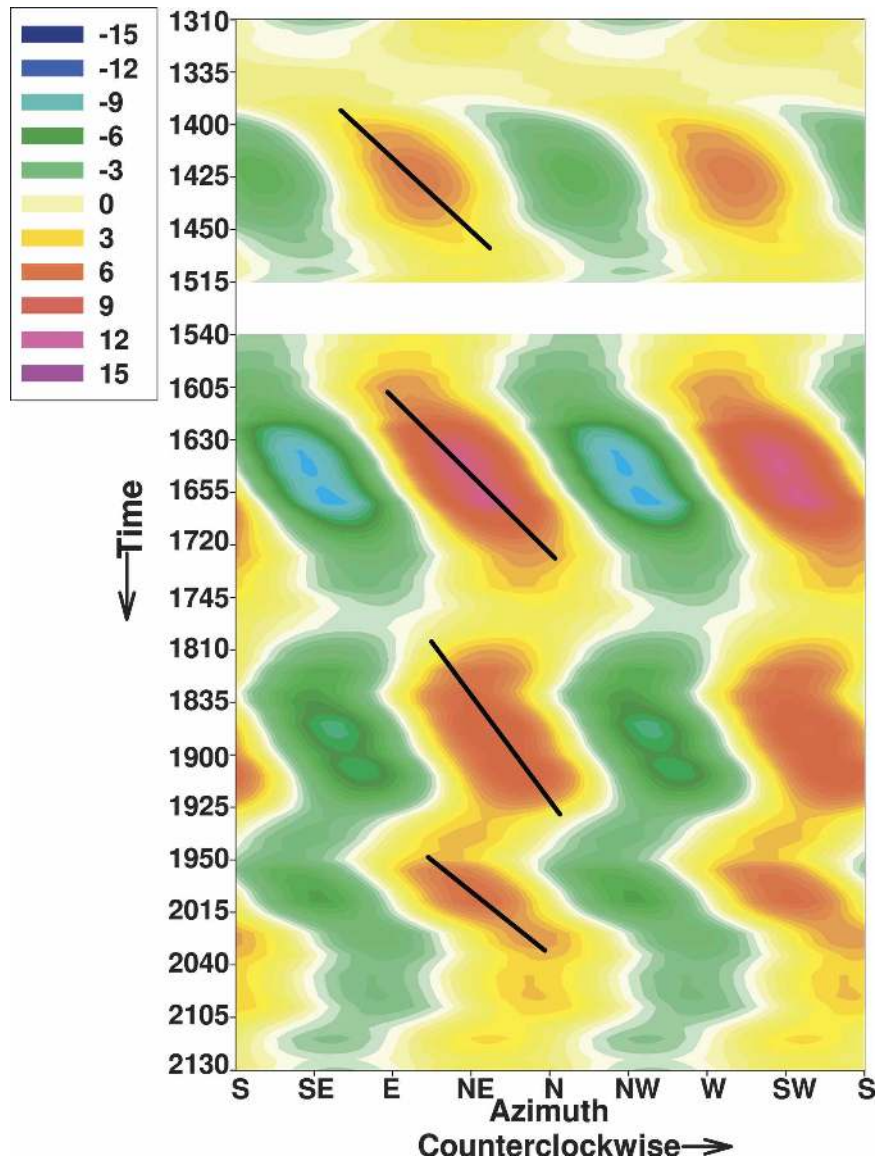


FIG. 10. Azimuth-time Hovmöller of the wavenumber 2 asymmetry 80 km from the center of Elena. The solid lines track the rotation of the wavenumber 2 asymmetries and inner spiral rainbands of Figs. 7 and 9.

elliptical eyewall and hypothesized mesovortices within the eye were noted to occur 3–4 h before Elena's period of rapid intensification came to an end; after which the storm slowly weakened prior to its landfall due to the circulation's proximity to land and ingestion of low- $\Theta_e$  air (Part I). Thus, even though the existence of mesovortices in Elena cannot be confirmed with the available data, the evolution of Elena's reflectivity, vorticity structure, and intensity late on 1 September is consistent with the barotropic instability mechanism of Schubert et al. (1999) and the observations of Reasor et al. (2000) and Kossin and Eastin (2001).

During this same time period, repeated bands of high reflectivity were noted to break off of the asymmetric deep convection in the northern eyewall (Figs. 4 and 7). These bands propagated outward and cyclonically around the storm into the southwest quadrant where deep convection was enhanced and they were seen to exhibit large amplitude in wavenumber 2 (Figs. 7 and 9). The magnitude of the wavenumber 2 asymmetry associated with the bands increased as they propagated outward between the 30- and 50-km radii (Figs. 7a–c). This growth was attributed to the presence of type II instability (Kossin et al. 2000) across the low-vorticity

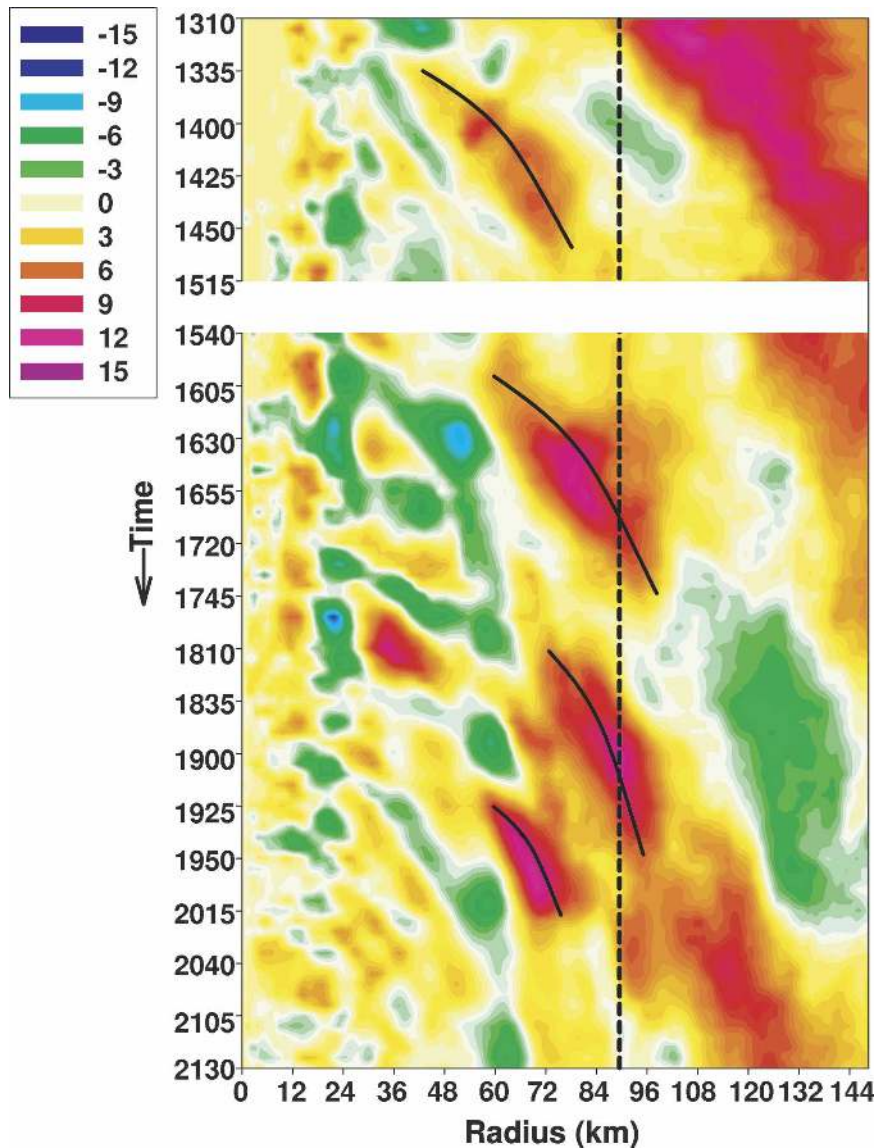


FIG. 11. Radius–time Hovmöller of the wavenumber 2 asymmetry along a radius drawn from the center of Elena toward the southwest. The solid curves track the outward propagation of the wavenumber 2 asymmetries and inner spiral rainbands of Figs. 7 and 9. The vertical dashed line is the stagnation radius.

moat located between the eyewall and an outer ring of enhanced vorticity (Fig. 8).

The bands had an average azimuthal velocity of  $25 \text{ m s}^{-1}$ , or  $\sim 68\%$  of the local tangential wind speed (Fig. 10), and an average outward radial velocity of  $5.2 \text{ m s}^{-1}$  (Fig. 11). The bands were noted to spiral outward to the  $\sim 100 \text{ km}$  radius where they began to thin and lose their convective signature (Fig. 7). The azimuthal and radial propagation speeds of the wavenumber 2 features, along with the existence of a wave stagnation radius, were found to be consistent with vortex Rossby wave theory (Montgomery and Kallenbach 1997).

Previous numerical modeling and observational studies have shown that VRWs could be the result of the expulsion of high vorticity from the eyewall during asymmetric mixing and vorticity rearrangement in the vortex due to barotropic instability (Schubert et al. 1999; Kossin et al. 2000). As detailed above, the evolution of Elena's reflectivity and vorticity structure indicates that barotropic instability was realized and asymmetric mixing did occur in the core of Elena. Additional support for this mechanism comes from the results of Reasor et al. (2000), who found that the most unstable wavenumber of the annular vorticity profile in

Olivia (1994) was wavenumber 2. They used this fact to conclude that the wavenumber 2 vorticity asymmetries, and associated spiral reflectivity bands seen outside the eyewall, were the natural by-product of the breakdown of the vorticity ring.

The eyewall breakdown and vorticity mixing argument for the generation of VRWs just described is an intrinsic part of the internal dynamics of the vortex, independent from the environment in which the storm is embedded. A second possible VRW formation mechanism is based on recent work by Reasor and Montgomery (2001) and Reasor et al. (2004). They showed that the interaction between a tropical cyclone and its environment via vertical wind shear also acts as a VRW generator. In their simulations, an originally vertically aligned dry vortex is exposed to and subsequently tilted by vertical wind shear. The tilt manifests itself as a wavenumber 1 PV anomaly that is dispersed as sheared VRWs that propagate outward and azimuthally around the storm. Although the vertical tilt of Elena was unable to be determined from the data collected, a strong wavenumber 1 asymmetry in reflectivity was noted (Figs. 3 and 4) and found to be forced by vertical wind shear. Furthermore, each of the four spiral rainbands with VRW characteristics documented in this study could be traced backward in time to convective features that broke off of and propagated away from this shear-forced asymmetric eyewall convection (Figs. 4c and 7e). This mechanism could lead to the formation of VRWs in the absence of barotropic instability.

**Acknowledgments.** The authors thank the research scientists from the Hurricane Research Division of NOAA for their dedicated efforts to collect the ground-based radar and reconnaissance flight data used for this study. We are indebted to David Vollaro for his help in developing computer programs to read and plot the reflectivity data, and to Lloyd Shapiro for his help in developing the azimuthal wavenumber decomposition. We would also like to thank James Kossin and an anonymous reviewer for their thoughtful comments that improved the quality of the manuscript. This work was supported by NSF Grants ATM0418682 and 0000673.

#### REFERENCES

- Black, M. L., J. F. Gamache, F. D. Marks Jr., C. E. Samsury, and H. E. Willoughby, 2002: Eastern Pacific Hurricanes Jimena of 1991 and Olivia of 1994: The effect of vertical wind shear on structure and intensity. *Mon. Wea. Rev.*, **130**, 2291–2312.
- Braun, S. A., 2002: A cloud-resolving simulation of Hurricane Bob (1991): Storm structure and eyewall buoyancy. *Mon. Wea. Rev.*, **130**, 1573–1592.
- Burpee, R. W., and M. L. Black, 1989: Temporal and spatial variations of rainfall near the centers of two tropical cyclones. *Mon. Wea. Rev.*, **117**, 2204–2218.
- Case, R. A., 1986: Atlantic hurricane season of 1985. *Mon. Wea. Rev.*, **114**, 1390–1405.
- Chen, Y., and M. K. Yau, 2001: Spiral bands in a simulated hurricane. Part I: Vortex Rossby wave verification. *J. Atmos. Sci.*, **58**, 2128–2145.
- , and —, 2003: Asymmetric structures in a simulated land-falling hurricane. *J. Atmos. Sci.*, **60**, 2294–2312.
- , G. Brunet, and M. K. Yau, 2003: Spiral bands in a simulated hurricane. Part II: Wave activity diagnostics. *J. Atmos. Sci.*, **60**, 1239–1256.
- Corbosiero, K. L., 2005: The structure and evolution of a hurricane in vertical wind shear. Ph.D. thesis, University at Albany, State University of New York, 148 pp.
- , J. Molinari, and M. L. Black, 2005: The structure and evolution of Hurricane Elena (1985). Part I: Symmetric intensification. *Mon. Wea. Rev.*, **133**, 2905–2921.
- Franklin, J. L., S. J. Lord, S. E. Feuer, and F. D. Marks Jr., 1993: The kinematic structure of Hurricane Gloria (1985) determined from nested analyses of dropwindsonde and Doppler radar data. *Mon. Wea. Rev.*, **121**, 2433–2451.
- Guinn, T. A., and W. H. Schubert, 1993: Hurricane spiral rainbands. *J. Atmos. Sci.*, **50**, 3380–3403.
- Jones, S. C., 1995: The evolution of vortices in shear. I: Initially barotropic vortices. *Quart. J. Roy. Meteor. Soc.*, **121**, 821–851.
- Knaff, J. A., J. P. Kossin, and M. DeMaria, 2003: Annular hurricanes. *Wea. Forecasting*, **18**, 204–223.
- Kossin, J. P., and M. D. Eastin, 2001: Two distinct regimes in the kinematic and thermodynamic structure of the hurricane eye and eyewall. *J. Atmos. Sci.*, **58**, 1079–1090.
- , and W. H. Schubert, 2001: Mesovortices, polygonal flow patterns, and rapid pressure falls in hurricane-like vortices. *J. Atmos. Sci.*, **58**, 2196–2209.
- , and —, 2004: Mesovortices in Hurricane Isabel. *Bull. Amer. Meteor. Soc.*, **85**, 151–153.
- , —, and M. T. Montgomery, 2000: Unstable interactions between a hurricane's primary eyewall and a secondary region of enhanced vorticity. *J. Atmos. Sci.*, **57**, 3893–3917.
- , B. D. McNoldy, and W. H. Schubert, 2002: Vortical swirls in hurricane eye clouds. *Mon. Wea. Rev.*, **130**, 3144–3149.
- , W. H. Schubert, C. Velden, M. Black, P. Black, R. Zehr, S. Aberson, and J. Dunion, 2004: Mesovortices in Hurricane Isabel (2003). Preprints, *26th Conf. on Hurricanes and Tropical Meteorology*, Miami, FL, Amer. Meteor. Soc., 447–448.
- Kuo, H.-C., R. T. Williams, and J.-H. Chen, 1999: A possible mechanism for the eye rotation of Typhoon Herb. *J. Atmos. Sci.*, **56**, 1659–1673.
- Lamb, H., 1932: *Hydrodynamics*. Dover, 732 pp.
- MacDonald, N. J., 1968: The evidence for the existence of Rossby-type waves in the hurricane vortex. *Tellus*, **20**, 138–150.
- Mallen, K. J., M. T. Montgomery, and B. Wang, 2005: Reexamining the near-core radial structure of the tropical cyclone primary circulation: Implications for vortex resiliency. *J. Atmos. Sci.*, **62**, 408–425.
- McWilliams, J. C., L. P. Graves, and M. T. Montgomery, 2003: A formal theory for vortex Rossby waves and vortex evolution. *Geophys. Astrophys. Fluid Dyn.*, **97**, 275–309.
- Möller, J. D., and M. T. Montgomery, 1999: Vortex Rossby waves and hurricane intensification in a barotropic model. *J. Atmos. Sci.*, **56**, 1674–1687.
- , and —, 2000: Tropical cyclone evolution via potential

- vorticity anomalies in a three-dimensional balance model. *J. Atmos. Sci.*, **57**, 3366–3387.
- , and L. J. Shapiro, 2002: Balanced contributions to the intensification of Hurricane Opal as diagnosed from a GFDL model forecast. *Mon. Wea. Rev.*, **130**, 1866–1881.
- Montgomery, M. T., and R. J. Kallenbach, 1997: A theory for vortex Rossby waves and its application to spiral bands and intensity changes in hurricanes. *Quart. J. Roy. Meteor. Soc.*, **123**, 435–465.
- , and J. Enagonio, 1998: Tropical cyclogenesis via convectively forced vortex Rossby waves in a three-dimensional quasigeostrophic model. *J. Atmos. Sci.*, **55**, 3176–3207.
- , H. D. Snell, and Z. Yang, 2001: Axisymmetric spindown dynamics of hurricane-like vortices. *J. Atmos. Sci.*, **58**, 421–435.
- Muramatsu, T., 1986: The structure of polygonal eye of a typhoon. *J. Meteor. Soc. Japan*, **64**, 913–921.
- Nolan, D. S., M. T. Montgomery, and L. D. Grasso, 2001: The wavenumber-one instability and trochoidal motion of hurricane-like vortices. *J. Atmos. Sci.*, **58**, 3243–3270.
- Reasor, P. D., and M. T. Montgomery, 2001: Three-dimensional alignment and corotation of weak, TC-like vortices via linear vortex Rossby waves. *J. Atmos. Sci.*, **58**, 2306–2330.
- , —, F. D. Marks Jr., and J. F. Gamache, 2000: Low-wavenumber structure and evolution of the hurricane inner core observed by airborne dual-Doppler radar. *Mon. Wea. Rev.*, **128**, 1653–1680.
- , —, and L. D. Grasso, 2004: A new look at the problem of tropical cyclones in vertical shear flow: Vortex resiliency. *J. Atmos. Sci.*, **61**, 3–22.
- Rogers, R., S. Chen, J. Tenerelli, and H. E. Willoughby, 2003: A numerical study of the impact of vertical wind shear on the distribution of rainfall in Hurricane Bonnie (1998). *Mon. Wea. Rev.*, **131**, 1577–1599.
- Schubert, W. H., M. T. Montgomery, R. K. Taft, T. A. Guinn, S. R. Fulton, J. P. Kossin, and J. P. Edwards, 1999: Polygonal eyewalls, asymmetric eye contraction, and potential vorticity mixing in hurricanes. *J. Atmos. Sci.*, **56**, 1197–1223.
- Senn, H. V., and H. W. Hise, 1959: On the origin of hurricane spiral rain bands. *J. Meteor.*, **16**, 419–426.
- Shapiro, L. J., and H. E. Willoughby, 1982: The response of balanced hurricanes to local sources of heat and momentum. *J. Atmos. Sci.*, **39**, 378–394.
- Swarztrauber, P. N., 1982: Vectorizing the FFTs. *Parallel Computations*, G. Rodrigue, Ed., Academic Press, 51–83.
- Tuttle, J. D., and B. Gall, 1995: Radar analysis of Hurricanes Andrew and Hugo. Preprints, *21st Conf. on Hurricanes and Tropical Meteorology*, Miami, FL, Amer. Meteor. Soc., 608–610.
- Wang, Y., 2001: An explicit simulation of tropical cyclones with a triply nested movable mesh primitive equation model: TCM3. Part I: Model description and control experiment. *Mon. Wea. Rev.*, **129**, 1370–1394.
- , 2002a: Vortex Rossby waves in a numerically simulated tropical cyclone. Part I: Overall structure, potential vorticity, and kinetic energy budgets. *J. Atmos. Sci.*, **59**, 1213–1238.
- , 2002b: Vortex Rossby waves in a numerically simulated tropical cyclone. Part II: The role in tropical cyclone structure and intensity changes. *J. Atmos. Sci.*, **59**, 1239–1262.
- , and G. J. Holland, 1996: Tropical cyclone motion and evolution in vertical wind shear. *J. Atmos. Sci.*, **53**, 3313–3332.
- Willoughby, H. E., and M. B. Chelmon, 1982: Objective determination of hurricane tracks from aircraft observations. *Mon. Wea. Rev.*, **110**, 1298–1305.
- , F. D. Marks Jr., and R. J. Feinberg, 1984: Stationary and moving convective bands in hurricanes. *J. Atmos. Sci.*, **41**, 3189–3211.